AD-753 077

CHEMICAL INJECTION INTO A REENTRY PLASMA TO IMPROVE HIGH POWER EM WAVE TRANSMISSION

Robert J. Papa

Air Force Cambridge Research Laboratories
L. G. Hanscom Field, Massachusetts

18 September 1972

DISTRIBUTED BY:

NTIS
National Technical Information Service
U. S. DEPARTMENT OF COMMERCE
5285 Port Royal Road, Springfield Va. 22151

AD753077

AFCRL-72-0556
18 SEPTEMBER 1972
PHYSICAL SCIENCES RESEARCH PAPERS, NO. 511

AIR FORCE CAMBRIDGE RESEARCH LABORATORIES
L. G. HANSCOM FIELD, BEDFORD, MASSACHUSETTS

Chemical Injection Into a Reentry Plasma to Improve High Power EM Wave Transmission

ROBERT J. PAPA

AIR FORCE SYSTEMS COMMAND
United States Air Force

35

Qualified requestors may obtain additional copies from the Defense Documentation Center. All others should apply to the National Technical Information Service.

A

Unclassified

Security Classification

DOCUMENT CONTROL DATA - R&D

(Security classification of title, body of abstract and indexing annotation must be entered when the overall report is classified)

1. ORIGINATING ACTIVITY (Corporate author) Air Force Cambridge Research Laboratories (LZ) L.G. Hanscom Field Bedford, Massachusetts 01730	2a. REPORT SECURITY CLASSIFICATION Unclassified 2b. GROUP

3. REPORT TITLE

CHEMICAL INJECTION INTO A REENTRY PLASMA TO IMPROVE HIGH POWER EM WAVE TRANSMISSION

4. DESCRIPTIVE NOTES (Type of report and inclusive dates)

Scientific. Interim.

5. AUTHOR(S) (First name, middle initial, last name)

Robert J. Papa

6. REPORT DATE 18 September 1972	7a. TOTAL NO. OF PAGES 33	7b. NO. OF REFS 30
8a. CONTRACT OR GRANT NO. b. PROJECT, TASK, WORK UNIT NOS. 5635-04-01 c. DOD ELEMENT 61102F d. DOD SUBELEMENT 681305	9a. ORIGINATOR'S REPORT NUMBER(S) AFCRL-72-0556 9b. OTHER REPORT NO(S) (Any other numbers that may be assigned this report) PSRP, No.511	

10. DISTRIBUTION STATEMENT

Approved for public release; distribution unlimited.

11. SUPPLEMENTARY NOTES TECH, OTHER	12. SPONSORING MILITARY ACTIVITY Air Force Cambridge Research Laboratories (LZ) L.G. Hanscom Field Bedford, Massachusetts 01730

13. ABSTRACT For purposes of electronic countermeasures, it is desirable to maximize the amount of power that can be transmitted from a reentry vehicle by suppressing the onset of antenna voltage breakdown. This can be accomplished by injecting chemicals into the reentry plasma sheath. This report describes a numerical procedure for calculating the amount of power that can be transmitted through a chemically seeded plasma. The power levels of a plane electromagnetic wave incident on a reentry plasma slab are sufficient to induce electron temperature changes. As a result, the electron density and effective collision frequency vary with time. The plasma properties are determined as a function of time by numerically solving three continuity equations and three momentum equations for the electrons, positive ions, and negative ions. The Poisson equation must be solved simultaneously with the above set of coupled, nonlinear, differential equations, since charge separation can occur in the plasma. The chemical processes of electron attachment, detachment, and recombination are included. Runge-Kutta numerical integration of Maxwell's equations together with the above set of plasma transport equations give the time-dependent plane wave transmission and reflection coefficients as a function of incident power level for a very wide range of reentry plasma conditions. The numerical results from such an analysis will permit the optimization of systems performance of high power antennas radiating through chemically seeded reentry flow fields.

DD FORM 1 NOV 65 1473

Unclassified

Security Classification

Ia

Unclassified

Security Classification

14. KEY WORDS	LINK A		LINK B		LINK C	
	ROLE	WT	ROLE	WT	ROLE	WT
Electronic countermeasures						
Reentry plasma						
Chemical injection						
Nonlinear EM wave propagation						

Unclassified

Security Classification

Ib

AFCRL-72-0556
18 SEPTEMBER 1972
PHYSICAL SCIENCES RESEARCH PAPERS, NO. 511

MICROWAVE PHYSICS LABORATORY PROJECT 5635

AIR FORCE CAMBRIDGE RESEARCH LABORATORIES

L. G. HANSCOM FIELD, BEDFORD, MASSACHUSETTS

Chemical Injection Into a Reentry Plasma to Improve High Power EM Wave Transmission

ROBERT J. PAPA

AIR FORCE SYSTEMS COMMAND
United States Air Force

II

Abstract

For purposes of electronic countermeasures, it is desirable to maximize the amount of power that can be transmitted from a reentry vehicle by suppressing the onset of antenna voltage breakdown. This can be accomplished by injecting chemicals into the reentry plasma sheath. This report describes a numerical procedure for calculating the amount of power that can be transmitted through a chemically seeded plasma. The power levels of a plane electromagnetic wave incident on a reentry plasma slab are sufficient to induce electron temperature changes. As a result, the electron density and effective collision frequency vary with time. The plasma properties are determined as a function of time by numerically solving three continuity equations and three momentum equations for the electrons, positive ions, and negative ions. The Poisson equation must also be solved simultaneously with the above set of coupled, nonlinear, differential equations, since charge separation can occur in the plasma. The chemical processes of electron attachment, detachment, and recombination are included. Runge-Kutta numerical integration of Maxwell's equations together with the above set of plasma transport equations give the time-dependent plane wave transmission and reflection coefficients as a function of incident power level for a very wide range of reentry plasma conditions. The numerical results from such an analysis will permit the optimization of systems performance of high power antennas radiating through chemically seeded reentry flow fields.

Contents

Illustrations

Preceding page blank

Chemical Injection Into a Reentry Plasma to Improve High Power EM Wave Transmission

1. INTRODUCTION

A high power electromagnetic wave radiating from a reentry vehicle will interact with the ionized flow field and create additional ionization. The additional ionization will result in severe signal attenuation and a drop in the transmitted power level. This phenomenon of antenna voltage breakdown constitutes a serious limitation on the capabilities of electronic countermeasures (ECM) systems. The ECM systems performance on hypersonic vehicles can be greatly improved by injecting electron-attaching chemicals into the reentry flow field. This report describes numerical procedures for solving the nonlinear plasma-transport equations coupled to Maxwell's equations, so that plane wave transmission and reflection coefficients can be calculated as a function of incident field strength.

When a radio frequency wave of sufficiently high intensity is applied to a partially ionized plasma, the electron density tends to increase in any region where the effective electron temperature is high enough to cause the ionization mechanisms to exceed the electron loss rates. Antenna voltage breakdown is said to occur when the electron density builds up to a critical value and the plasma layer covering the radiating system becomes thick enough so that the power is almost entirely absorbed or reflected, with relatively little transmission.

(Received for publication 18 September 1972)

Many papers and several books have been devoted to the problem of determining the threshold required to produce antenna breakdown for a given geometrical configuration and a given set of ambient conditions (Epstein and Lenander, 1968; Lenander, 1968a, b; MacDonald et al, 1963; Epstein, 1965, 1968; Taylor et al, 1968; Light and Taylor, 1968; Fante, 1971; Fante and Mullin, 1965; Mayhan and Fante, 1969; MacDonald, 1966). Breakdown of a gas may be either on a pulsed or CW basis. In pulsed breakdown, the electron density must reach some critical value before the end of the pulse. In the references cited, various geometrical configurations for the electric field were considered, such as (1) parallel plates, (2) a cylindrical cavity, and (3) a slot antenna on a ground plane.

The theoretical analysis of gas breakdown is usually based on either a phenomenological model or the more rigorous Boltzmann equation approach. The phenomenological approach is based on the criterion that the electron gain terms just barely exceed the electron loss terms in the continuity equation. The reaction rate coefficients that appear in the electron continuity equation are considered to be functions of an effective electric field, E_e. As indicated by MacDonald (1966), the effective electric field concept is strictly valid only for gases in which the electron-neutral collision frequency ν_{eN} is a constant:

$$E_e = \left[E^2/(1 + \omega^2/\nu_{eN}^2)\right]^{1/2} \qquad (1)$$

where E = electric field amplitude, E_e = effective electric field, ω = signal frequency, and ν_{eN} = electron-neutral collision frequency.

As illustrated on p. 171 of MacDonald (1966), the effective field concept for a gas mixture like air with velocity dependent collision frequencies becomes ambiguous at low gas pressures.

The more rigorous approach to gas breakdown involves the solution of the Boltzmann equation for the electron distribution function. In the case of a gas mixture subjected to an intense a-c electric field, there are several computer programs available for solving the Boltzmann equation numerically. The determination of the electron distribution function enables the transport coefficients and reaction rate coefficients to be accurately determined as a function of gas composition, signal frequency, and electric field intensity. Once the transport coefficients are known as a function of electric field intensity, gas pressure p, and signal frequency ω, then, for a fixed gas composition and uniform electric field, the breakdown threshold can be determined graphically (MacDonald, 1966, p. 179 et seq.). For nonuniform electric field distributions, Epstein (1968) and Mayhan and Fante (1969) solve for the breakdown field strength by using variational techniques. An excellent review of the field of voltage breakdown of microwave antennas was presented by Taylor et al (1971).

In addition to the problem of determining the power level at which breakdown occurs, from an ECM systems point of view it is also important to calculate the amount of power that can be transmitted through a reentry plasma sheath before, during, and after breakdown. Several papers have dealt with the probem of nonlinear propagation of high power EM waves through the ionized flow field of a reentry vehicle: Papa and Case, 1965; Mayhan and DeVore, 1968; Epstein, 1969; Mayhan, 1969; Fante, 1971; and Fante and Mayhan, 1971. Except for the work of Fante (1971), who made certain assumptions about the smallness of the temperature and pressure gradients in the gas, all of these papers rely on computer solutions of the electron continuity equation coupled with Maxwell's equations to determine the nonuniform field distribution and power transmitted through a one-dimensional plasma slab. Flow-field data are used to furnish the initial electron temperature, gas temperature, and electron density distributions in the plasma slab.

This report is an extension of previous work to the case where negative ions are present in the reentry plasma sheath. The processes of electron attachment, electron detachment, and positive-ion negative-ion recombination must be considered. The diffusion process, which is free electron diffusion at low electron densities and ambipolar diffusion at high electron densities, is altered by the presence of the negative ions. Thus, because of charge separation in the time-varying plasma, Poisson's equation for the internal plasma field must be solved simultaneously with three continuity equations and three momentum equations for the electrons, positive ions, and negative ions. These seven plasma-transport equations contain coefficients (transport coefficients) that are functions of the electron velocity distribution function, f. Another computer program solves the Boltzmann equation for the electron distribution function for a given set of neutral gas conditions, such as gas temperature, pressure, and composition. In addition to being a function of the gas composition, f is also a function of the a-c field intensity E and the signal frequency ω.

The geometry of the EM wave-plasma interaction is indicated in Figure 1. The gas composition and neutral gas temperature T vary only in the x direction. Thus, for a fixed signal frequency, the electron distribution function f depends on x (the local gas temperature and composition) and E (the local a-c field intensity); consequently, the transport coefficients are functions of x and E.

The solution of the nonlinear propagation problem is started by first integrating Maxwell's equations step-by-step backward through the slab, using a fourth-order Runge-Kutta technique. Since the ratio of the a-c electric field to the a-c magnetic field can be assumed on the transmitted face of the slab ($x = L$), the initial field distribution in the slab can be determined. This fixes the transport coefficients at one instant in time ($t = 0$). Then, the continuity equations for each charged

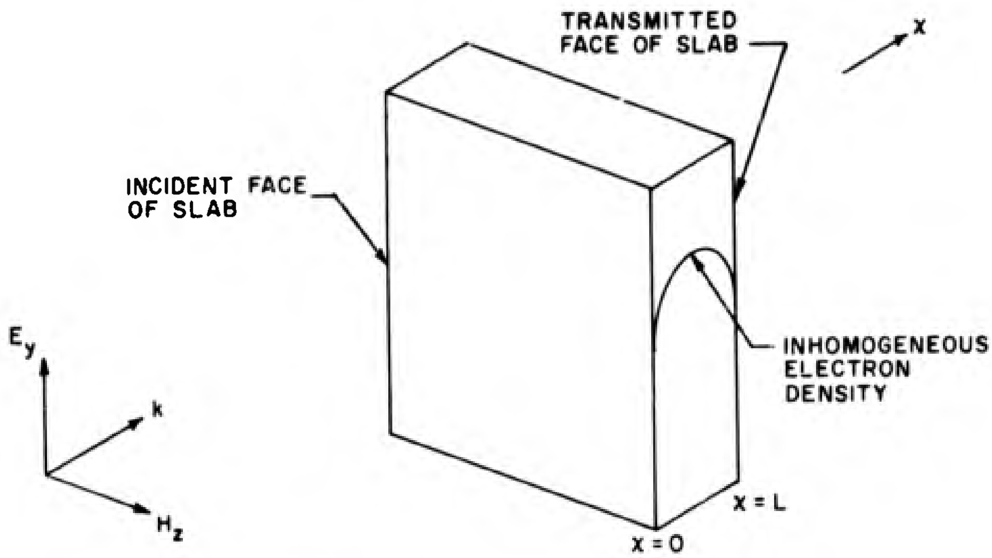

Figure 1. Plane Wave Incident on Inhomogeneous Reentry Plasma Sheath

species may be integrated a small increment forward in time, again using a fourth-order Runge-Kutta method.

The new electron temperature and density profiles fix a new set of values for the complex dielectric constant of the plasma, $K = K(x)$, at time $t = \Delta t$. Then, Maxwell's equations are integrated backward through the slab, holding $K(x)$ and the electron temperature $T_e(x)$ fixed (independent of E).

Since the incident field amplitude E_{INC} must remain fixed, a value for the total electric field and total magnetic field can be calculated on the incident face of the slab. Then, Maxwell's equations are integrated forward through the slab, where the real and imaginary parts of $K(x)$ are allowed to vary as a function of E at each forward step of the integration procedure. The backward integration procedure is resumed, using the latest variation of K with x determined from the previous forward integration procedure.

The backward and forward integrations of Maxwell's equations through the slab are iterated until the successive variations in the field distribution fall below a pre-assigned tolerance. This permits the electron temperature profile $T_e(x)$ to be calculated for a particular instant of time. A new determination of the transport coefficients as a function of x then allows the continuity equations to be calculated at another forward increment in time.

The entire procedure is then reiterated until the electromagnetic transmission coefficient becomes much smaller than one, indicating that the plasma sheath has become very overdense. If the incident power level is not so high that it can cause almost total loss of transmission, the transmission coefficient will at first decrease somewhat and then incline to a new steady value. It is conceivable to find plasma conditions where the transmission coefficient can actually increase as the incident power is increased, but in any situation, for a sufficiently long time, the transmission coefficient will become independent of time (for a CW signal).

2. THE PLASMA TRANSPORT EQUATIONS COUPLED WITH MAXWELL'S EQUATIONS

In order to render the problem of high power EM waves interacting with a chemically seeded plasma tractable, it is necessary to make a number of simplifying assumptions. The most important of these assumptions are the following:

1. There is no variation of the plasma parameters in the y or z direction (see Figure 1), $\partial/\partial y = \partial/\partial z = 0$, there is variation only in the x-direction.

2. The positive and negative ion temperatures are equal to the neutral gas temperature T, which remains constant.

3. There is no heat flux in the electron gas.

4. There are no plasma radiation effects on the excitation of atomic states or on the ionization mechanisms.

5. The incident wave is a plane wave at normal incidence on the plasma slab.

6. The electron pressure tensor $\Psi_{ij}^{(e)}$ is isotropic:

$$\Psi_{ij}^{(e)} = P^{(e)} \delta_{ij} .$$

7. There is no d-c magnetic field present.

8. There is no effect on the plasma processes due to metastable states, nor are there any inelastic collisions of the second kind.

9. The neutral gas has no net mean velocity.

10. The plasma is nonrelativistic, so that the effect of the a-c magnetic field is negligible compared to the a-c electric field.

11. The isotropic part of the electron distribution function is nearly Maxwellian, so that an effective electron temperature T_e can be defined.

12. The time scale for electron temperature changes τ_T is shorter than the time scale for electron density changes τ_N, so that the electron temperature has time to reach a quasi-steady state before the electron density starts to change.

In the present analysis, the plasma is described by three continuity equations and three momentum equations, plus Poisson's equation for the self-consistent electric field in the plasma. These transport equations, when coupled with

Maxwell's equations, are used to describe the nonlinear EM transmission of waves through the plasma. However, this set of equations is not complete, because there is no equation governing the electron temperature. Instead of including a separate equation for determining the electron temperature, it is more accurate, and convenient, to employ another separate computer program for determining the electron velocity distribution function f. This separate computer program was written originally by Carleton and Megill (1962). An updated version of the program was made by Lenander (1968b) for studying the effects of ablation products on RF breakdown in the boundary layer of a hypersonic flow field. The computer program is being further generalized at AVCO by Mayan and Yos (1969). The listing and source decks for this program are now available for use on the AFCRL CDC 6600.

The Boltzmann equation program solves the electron Boltzmann equation numerically to obtain the steady state electron distribution function f in a slightly ionized gas under the influence of a strong a-c electric field. Both elastic and inelastic collision processes are included in the program, using realistic collision cross section data from a binary data tape containing provisions for storing up to 100 species, with up to 20 different collision processes per species. Since the neutral gas temperature and composition are known as a function of x (see Figure 1) from flow field calculations, it is possible to break the reentry plasma slab into a number of layers (about 12) and to solve for f at a fixed frequency, as a function of electric field E, for a number of x values.

The computer program then averages the appropriate cross section over the distribution function to obtain the following transport coefficients: ionization frequency due to electron impact on neutrals ν_I, real and imaginary parts of the plasma dielectric constant $K = K_R + iK_I$, and the average electron energy u_{AV}. For a given signal frequency ω, the values of ν_I, K_R, K_I, and u_{AV} are calculated for about 10 values of E in each layer of the plasma slab (12 layers, corresponding to 12 values of x from $x = 0$ to $x = L$). The calculated values of ν_I, K_R, K_I, and u_{AV} as a function of E and x are stored in the nonlinear transmission program as two-dimensional arrays. When these quantities are required at intermediate values of E or x, very accurate spline interpolation routines are used.

Under the 12 assumptions previously stated, the plasma transport equations coupled with Maxwell's equations may be written:

$$\frac{\partial E_y}{\partial x} + \mu_0 \frac{\partial H_z}{\partial t} = 0 \tag{1}$$

$$\frac{\partial H_z}{\partial x} + \epsilon_0 \frac{\partial E_y}{\partial t} - e N_e v_y + e N_I V_y^I - e N_{NI} V_y^{NI} = 0 \tag{2}$$

$$\frac{\partial N_e}{\partial t} = (\nu_I - \nu_a - \nu_{DR} N_I) N_e + I + \nu_{DET} N_{NI} - \frac{\partial \Gamma_e}{\partial x} \quad (3)$$

$$\frac{\partial N_I}{\partial t} = I + \nu_I N_e - (\nu_{DR} N_e + \alpha_r N_{NI}) N_I - \frac{\partial \Gamma_I}{\partial x} \quad (4)$$

$$\frac{\partial N_{NI}}{\partial t} = \nu_a N_e - \alpha_r N_{NI} N_I - \nu_{DET} N_{NI} - \frac{\partial \Gamma_{NI}}{\partial x} \quad (5)$$

$$\frac{\partial (N_e v_x)}{\partial t} + \frac{\partial (N_e v_x^2)}{\partial x} + \frac{1}{m} \frac{\partial (N_e k T_e)}{\partial x} + N_e \left(\frac{e}{m}\right) E_x =$$

$$- N_e \nu_{eN} v_x + N_e \nu_{eI} (V_x^I - v_x) + N_e \nu_{eNI} (V_x^{NI} - v_x) \quad (6)$$

$$\frac{\partial (N_I V_x^I)}{\partial t} + \frac{\partial (N_I {V_x^I}^2)}{\partial x} + \frac{1}{m_I} \frac{\partial (N_I k T)}{\partial x} - N_I \left(\frac{e}{m_I}\right) E_x = -N_I \left(\frac{\nu_{IN} m_N}{m_I + m_N}\right) V_x^I$$

$$+ N_I \left(\frac{m}{m_I}\right) \nu_{eI} (v_x - V_x^I) + N_I \left(\frac{m_{NI}}{m_I + m_{NI}}\right) \nu_{INI} (V_x^{NI} - V_x^I) \quad (7)$$

$$\frac{\partial (N_{NI} V_x^{NI})}{\partial t} + \frac{\partial (N_{NI} {V^{NI}}^2)}{\partial x} + \frac{1}{m_{NI}} \frac{\partial (N_{NI} k T)}{\partial x} + N_{NI} \left(\frac{e}{m_{NI}}\right) E_x =$$

$$- N_{NI} \left(\frac{\nu_{NIN} m_I}{m_{NI} + m_I}\right) V_x^{NI} + N_{NI} \left(\frac{m}{m_{NI}}\right) \nu_{NIe} (v_x - V_x^{NI})$$

$$+ N_{NI} \left(\frac{m_I}{m_I + m_{NI}}\right) \nu_{NII} (V_x^I - V_x^{NI}) \quad (8)$$

$$\frac{\partial E_x}{\partial x} = \left(\frac{e}{\epsilon_0}\right) \left[N_I - N_e - N_{NI}\right] . \quad (9)$$

The symbols appearing in the nine equations are defined as follows:

E_y = a-c electric field amplitude

μ_0 = permeability of free space

H_z = a-c magnetic field intensity

ϵ_0 = permittivity of free space

v_y = y-component of electron velocity

V_y^I = y-component of positive ion velocity

V_y^{NI} = y-component of negative ion velocity

N_e = electron density

N_I = positive ion density

N_{NI} = negative ion density

v_x = x-component of electron velocity

e = electron charge

k = Boltzmann's constant

T = neutral gas temperature

T_e = electron temperature

E_x = self-consistent quasi-static electric field due to charge separation

m = electron mass

m_N = neutral particle mass

m_I = ion mass

m_{NI} = negative ion mass

ν_{eN} = electron-neutral collision frequency

ν_{eI} = electron-ion collision frequency

ν_{eNI} = electron-negative ion collision frequency

ν_{INI} = ion-negative ion collision frequency

ν_I = ionization frequency due to electron impact on neutrals

ν_a = electron attachment frequency

ν_{DR} = dissociative recombination rate constant

I = ionization rate due to associative ionization

ν_{DET} = electron detachment rate constant

Γ_e = electron flux in x-direction

Γ_e = $N_e v_x$

Γ_I = ion flux in x-direction

$\Gamma_I \quad = N_I V_x^I$

$\Gamma_{NI} \quad$ = negative ion flux in x-direction

$\Gamma_{NI} \quad = N_{NI} V_x^{NI}$

$\alpha_r \quad$ = recombination rate constant for ion-ion recombination.

In the plasma transport equations, the following chemical reactions are included in the analysis:

Ionization Mechanisms: Associative Ionization

$$N + O \rightarrow NO^+ + e \tag{10}$$

$$k_{AI} = \frac{(0.518)\exp(-0.319 \times 10^5/T)}{6.025(10^{17})} \quad \frac{\text{meters}^3}{\text{particle-sec}} \quad .$$

Electron-Neutral Impact Ionization

$$e + X \rightarrow X^+ + 2e \quad . \tag{11}$$

The ν_I is calculated from Boltzmann equation program as a function of E and x.

Recombination Mechanisms: Dissociative Recombination

$$e + NO^+ \rightarrow N + O \tag{12}$$

$$\nu_{DR} = \frac{0.144(T_e^{-3/2})}{6.025(10^7)} \quad \frac{\text{meters}^3}{\text{particle-sec}} \quad .$$

Ion-Ion Recombination

$$X^- + M^+ + Y \rightarrow X + M + Y \tag{13}$$

$$\alpha_r = \frac{0.015(10^{-6})(N k T)}{T^{5/2}} \quad \frac{\text{meters}^3}{\text{particle-sec}}$$

N = total neutral density

T = gas temperature.

Attachment Mechanisms

$$Q + e \rightarrow F^- + \text{products} \tag{14}$$

$$\nu_{AT} = (N_{NI})0.3(10^{-7})\ T_e^{-2}\ (1/\text{sec})$$

Q = Freon E-3

N_{NI} = negative ion density in particles/m^3.

Detachment Mechanisms

$$F^- + M \rightarrow F + e + M \ \frac{\text{meters}^3}{\text{particle-sec}} \tag{15}$$

$$\nu_{DET} = N\ (3)\ (10^{-10})\ \exp\left(\frac{(-80000)}{1.98T}\right)\ (1/\text{sec})$$

N = total neutral density in particles/m^3.

These values for the reaction rate coefficients were taken from Lew (1970) and Pergament et al (1972). It can be shown from kinetic theory that when the reactants in a chemical reaction do not involve the electrons, the reaction rate constant is a function of the gas temperature; if one of the reactants is an electron, the rate coefficient is a function of the electron temperature. The electron-neutral collision frequency ν_{eN} for electrons colliding with each of the constituents of high temperature air was evaluated by integrating the data presented in the paper by Shkarofsky et al (1961) over a Maxwellian distribution function. The collision frequency for positive ions colliding with each neutral constituent ν_{IN} was obtained from the formula

$$\nu_{IN} = \frac{(kT)p}{\mu(D_{I,N}p)} \tag{16}$$

where

T = gas temperature

p = gas pressure

$$\mu = \frac{m_I m_N}{m_I + m_N} = \text{reduced mass}$$

and $D_{I,N}$ = diffusion coefficient for positive ions (NO^+) diffusing into a neutral gas (N).

The following values for $(D_{IN}p)$ are taken from Lew (1972):

$$(D_{I,NO}p) = e^{-11.442}\left[T^{(0.003993\, \ln T + 1.5689)}\right] \frac{cm^2\text{-}atm}{sec} \tag{17}$$

$$(D_{I,N}p) = e^{-12.978394}\left[T^{(0.0003467\, \ln T + 1.8941)}\right] \frac{cm^2\text{-}atm}{sec} \; . \tag{18}$$

The reaction rates listed in Eqs. (10) through (15) are selected so as to include only the dominant chemical reactions. Thus, the charged species O^+, N^+, O_2^+, and N_2^+ have been neglected in comparison to the charged species NO^+. This is a reasonable assumption, since NO has a lower ionization potential than any other neutral constituent. Therefore, to the original 12 assumptions the following assumptions must be added:

13. NO^+ is the only positive ion present in the plasma.

14. The electron attaching substance is assumed not to decompose or to react with the other neutral constituents. (This assumption is added to reduce the great complexity of the reaction rate chemistry.)

It is important to note that in the second Maxwell Eq. (2), the total current density J is composed of three terms: a current density due to electron motion $-e\,N_e\,v_y$, a current density due to positive ion motion $e\,N_I\,V_y^I$, and a current density due to negative ion motion $-e\,N_{NI}\,V_y^{NI}$. The electron current density is obtained from the relation

$$J_e = -e\,N_e\,v_y = -e\int f v_y\, d^3v = (i\omega\epsilon_0)(1-K)E_y \tag{19}$$

where K = complex dielectric constant and it is assumed that $E_y \sim \exp(-i\omega t)$.

The Boltzmann equation computer program gives values for K at a fixed ω as a function of E and x. If, for the moment, the electron-neutral collision frequency ν_{eN}, the electron-ion collision frequency ν_{eI}, and the electron-negative ion collision frequency are all assumed to be constant, the equation for the y-component of the electron velocity would be:

$$\frac{\partial(N_e v_y)}{\partial t} + \frac{\partial(N_e v_x v_y)}{\partial x} + N_e\left(\frac{e}{m}\right)E_y = -N_e \nu_{eN} v_y + N_e \nu_{eI}(V_y^I - v_y)$$

$$- N_e \nu_{eNI}\,(V_y^{NI} - v_y)\; . \tag{20}$$

From the equations for V_y^I and V_y^{NI} corresponding to Eq. (20), it can be shown that V_y^I and V_y^{NI} can be neglected compared to v_y if the following two assumptions are made:

15. $m_I(\nu_{IN}) >> m\,\nu_{eN}$

16. $m_{NI}(\nu_{NIN}) >> m\,\nu_{eN}$.

Thus, under assumptions 15 and 16, the total current density J is given by the electron current density as expressed in Eq. (19).

Another important fact is that Eq. (19) is strictly valid only when the terms $v_y \frac{\partial N_e}{\partial t}$ and $\frac{\partial(N_e v_x v_y)}{\partial x}$ are small compared to $N_e\,\nu_{eN}\,v_y$ in Eq. (20). This is true under the following assumptions:

17. The time scale for electron density changes τ_N is large compared to a wave period $(2\pi/\omega)$:

$$\tau_N >> (2\pi/\omega) .$$

18. The electron-neutral collision frequency ν_{eN} is large compared to v_D/L_{N_e}, where v_D is the drift velocity of the electrons in the x direction and L_{N_e} is the space scale for electron density changes:

$$\nu_{eN} >> v_D/L_{N_e} .$$

19. The signal frequency is large compared to v_D/L_{N_e} :

$$\omega >> v_D/L_{N_e} .$$

Under assumptions 15 through 19, the two Maxwell's Eqs. (1) and (2) now become

$$\frac{\partial E_y}{\partial x} - i\omega\mu_0 H_z = 0 \tag{21}$$

$$\frac{\partial H_z}{\partial x} - i\omega\epsilon_0 K E_y = 0 \tag{22}$$

where E_y and $H_z \sim \exp(-i\omega t)$.

The three continuity Eqs. (3), (4), and (5) will not be further simplified.

Further simplifications of the three momentum Eqs. (6), (7), and (8) are necessary for purposes of numerical tractability and feasibility of solution. It is desirable to eliminate the three time-derivative terms

$$\frac{\partial (N_e v_x)}{\partial t}, \quad \frac{\partial (N_I V_x^I)}{\partial t}, \quad \text{and} \quad \frac{\partial (N_{NI} V_x^{NI})}{\partial t}$$

from Eqs. (6), (7), and (8). This may be accomplished by making the following three assumptions:

20. The electron density time scale τ_N is large compared to $(1/\nu_{en})$:

$$\tau_N >> 1/\nu_{en} .$$

21. The ion density time scale τ_{NI} is large compared $(1/\nu_{IN})$:

$$\tau_{NI} >> 1/\nu_{IN} .$$

22. The negative ion density time scale $\tau_{N_{NI}}$ is large compared to $(1/\nu_{en})$:

$$\tau_{N_{NI}} >> 1/\nu_{NIN} .$$

Another crucial simplification of the three momentum equations occurs if they can be uncoupled from each other. This uncoupling can be achieved if six additional assumptions are made concerning the order of magnitude of the collision frequencies:

23. The electron-neutral collision frequency ν_{eN} is large compared to the electron-ion collision frequency ν_{eI}:

$$\nu_{eN} >> \nu_{eI} .$$

24. The electron-neutral collision frequency ν_{eN} is large compared to the electron-negative ion collision frequency ν_{eNI}:

$$\nu_{eN} >> \nu_{eNI} .$$

25. The ion-neutral collision frequency ν_{IN} is large compared to $(m/m_I)\,\nu_{eI}$:

$$\nu_{IN} >> (\dot{m}/m_I)\,\nu_{eI} .$$

26. The ion-neutral collision frequency ν_{IN} is large compared to the quantity $\frac{m_{NI}}{m_I + m_{NI}} \nu_{INI}$:

$$\nu_{IN} >> \left(\frac{m_{NI}}{m_I + m_{NI}}\right) \nu_{INI} .$$

27. The negative ion-neutral collision frequency ν_{NIN} is large compared to $(m/m_{NI})\, \nu_{NIe}$:

$$\nu_{NIN} >> (m/m_{NI})\, \nu_{NIe} .$$

28. The negative ion-neutral collision frequency ν_{NIN} is large compared to $\left(\frac{m_I}{m_I + m_{NI}}\right) \nu_{NII}$:

$$\nu_{NIN} >> \left(\frac{m_I}{m_I + m_{NI}}\right) \nu_{NII} .$$

The nonlinear convective derivative terms $\frac{\partial (N_e v_x^2)}{\partial x}$, $\frac{\partial (N_I V^{I^2})}{\partial x}$, and $\frac{\partial (N_{NI} V_x^{NI^2})}{\partial x}$ in the three momentum equations also should be eliminated for further simplification. These terms can be eliminated under the following three assumptions:

29. The electron-neutral collision frequency ν_{eN} is large compared to v_0/L_{N_e}, where v_D is the electron drift velocity in the x-direction and L_{N_e} is the scale length for electron density changes.

30. The ion-neutral collision frequency ν_{IN} is large compared to V_D^I/L_{N_I}, where V_D^I is the ion drift velocity in the x-direction and L_{N_I} is the scale length for ion density changes.

31. The negative ion-neutral collision frequency ν_{NIN} is large compared to $v_D^{NI}/L_{N_{NI}}$, where v_D^{NI} is the negative ion drift velocity in the x-direction and $L_{N_{NI}}$ is the scale length for negative ion density changes.

The effective collision frequency ν_{eff} and effective plasma frequency $\omega_{P_{eff}}$ were first defined by Whitmer and Herrmann (1966) and later generalized by Bakski et al (1968). These effective parameters of a plasma are defined in terms of the real part of the electrical conductivity σ_R and the imaginary part of the electrical conductivity σ_I as follows:

$$\nu_{eff} = \omega\left(\frac{\sigma_R}{\sigma_I}\right) \tag{23}$$

$$\omega^2_{P_{eff}} = \left(\frac{\omega}{\epsilon_0}\right)\left[\frac{\sigma_R^2 + \sigma_I^2}{\sigma_I}\right] . \tag{24}$$

The complex dielectric constant of the plasma K is related to the conductivity σ in the following manner:

$$K = 1 + \frac{i\sigma}{\omega\epsilon_0} . \tag{25}$$

A parameter ρ may be conveniently defined as the ratio of effective plasma frequency squared $\omega^2_{P_{eff}}$ to the actual plasma frequency squared ω_P^2:

$$\rho = \left(\omega^2_{P_{eff}} / \omega^2_P\right) \tag{26}$$

where

$$\omega_P^2 = N_e e^2/(m\epsilon_0) .$$

Using Eqs. (23) through (26) and restricting the nonlinear EM wave-plasma interaction to conditions where the 31 assumptions are valid, the plasma transport equations coupled to the Maxwell's equations take the form:

$$\frac{\partial E_R}{\partial x} = -\omega\mu_0 H_I \tag{27}$$

$$\frac{\partial E_I}{\partial x} = \omega\mu_0 H_R \tag{28}$$

$$\frac{\partial H_R}{\partial x} = -\omega\epsilon_0 E_I - \frac{N_e e^2 E_R \nu_{eff}\rho}{m(\omega^2 + \nu^2_{eff})} + \frac{N_e e^2 E_I \omega}{m(\omega^2 + \nu^2_{eff})} \tag{29}$$

$$\frac{\partial H_I}{\partial x} = \omega\epsilon_0 E_R - \frac{N_e e^2 E_R \omega\rho}{m(\omega^2 + \nu^2_{eff})} - \frac{N_e e^2 E_I \nu_{eff}\rho}{m(\omega^2 + \nu^2_{eff})} \tag{30}$$

$$-\frac{\partial N_e}{\partial t} = (\nu_I - \nu_a - \nu_{DR} N_I) N_e + I + \nu_{DET} N_{NI} - \frac{\partial \Gamma_e}{\partial x} \tag{31}$$

$$\frac{\partial N_I}{\partial t} = I + \nu_I N_e - (\nu_{DR} N_e + \alpha_r N_{NI}) N_I - \frac{\partial \Gamma_I}{\partial t} \tag{32}$$

$$\frac{\partial N_{NI}}{\partial t} = \nu_a N_e - \alpha_r N_{NI} N_I - \nu_{DET} N_{NI} - \frac{\partial \Gamma_{NI}}{\partial x} \tag{33}$$

$$\Gamma_e = \left(\frac{k}{m\nu_{en}}\right) \frac{\partial (N_e T_e)}{\partial x} - \frac{N_e e}{m\nu_{en}} E_x \tag{34}$$

$$\Gamma_I = \left(\frac{-k}{m_I \nu_{IN}}\right) \frac{\partial (N_i T)}{\partial x} + \frac{N_I e}{m_I \nu_{IN}} E_x \tag{35}$$

$$\Gamma_{NI} = \left(- \frac{k}{m_{NI} \nu_{NIN}}\right) \frac{\partial (N_{NI} T)}{\partial x} - \frac{N_{NI} e}{m_{NI} \nu_{NIN}} E_x \tag{36}$$

$$\frac{\partial E}{\partial x} = \left(\frac{e}{\epsilon_0}\right) \left[N_I - N_e - N_{NI}\right] . \tag{37}$$

Here, E_R = REAL (E_y), E_I = IMAG (E_y), etc.

The 11 Eqs. (27) through (37) are to be solved numerically together with the Boltzmann equation computer program data giving $T_e = T_e(E, x)$, $\nu_I = \nu_I(E, x)$, $\nu_{eff} = \nu_{eff}(E, x)$ and $\rho = \rho(E, x)$, where $E = \sqrt{E_R^2 + E_I^2}$.
The equations are to be solved subject to the initial and boundary conditions:

$N_e(x, t = 0)$ given for $0 \le x \le L$,

$N_I(x, t = 0)$ given for $0 \le x \le L$,

N_{NI}, $(x, t = 0)$ given for $0 \le x \le L$,

E_R, E_I, H_R, H_I given at $x = L$,

T_e $(x, t = 0)$ given for $0 \le x \le L$,

and $E_x(x = 0)$ given for all time.

The wall at $x = 0$ is assumed to be catalytic, so that $N_e(x = 0) = N_I(x = 0) = N_{NI}(x = 0) = 0$ and $T_e(x = 0) = T$ for all time t. Thus, to the 31 previous assumptions, one additional assumption must be added:

32. At the wall ($x = 0$) corresponding to a reentry vehicle surface, all the charged species recombine ($N_e = N_I = N_{NI} = 0$) and there is no Langmuir-Child plasma sheath formation.

3. NUMERICAL METHODS OF SOLUTION

The numerical solution of the coupled set of nonlinear Eqs. (27) through (37) involves three stages, which are repeated a specified number of times. The first stage is the numerical integration of Maxwell's equations step-by-step backward through the slab from $x = L$ to $x = 0$ (see Figure 1). This allows the complex impedance of the slab Z, the complex reflection coefficient R, and the complex transmission coefficient TR to be evaluated. The incident electric field E_{INC} remains constant, so that the total electric field at the incident face of the slab E_y ($x = 0$) can be determined from the relation $E_y (x = 0) = (1.0 + R) E_{INC}$. The total magnetic field on the incident face of the slab H_z ($x = 0$) can be calculated from the relation $H_z (x = 0) = E_y (x = 0)/Z$.

The second stage is the forward integration of Maxwell's equations step-by-step through the slab from $x = 0$ to $x = L$. At each step of the integration procedure, the effective collision frequency ν_{eff} (E, x) and normalized effective plasma frequency squared ρ (E, x) are evaluated at each point, where the total electric field is assumed to remain constant across each little layer of plasma. This is a good approximation, since the step size in the integration procedure is taken to be less than 0.01 times the free space wavelength. The backward integration of Maxwell's equations is then resumed, using the most recent values for ν_{eff} (E, x) and ρ(E, x), which were evaluated from the previous forward integration of Maxwell's equations. The result of a second backward integration of Maxwell's equations through the slab permits new values to be calculated for R, TR, and Z. Then, since E_{INC} remains constant, new values for $E_y(x = 0)$ and H_z ($x = 0$) can be evaluated. The backward and forward integrations of Maxwell's equations through the slab must be reiterated until the electric field distribution on two successive forward integrations differs by less than a preassigned tolerance.

The third stage in the numerical solution involves the evaluation of all the quantities on the right-hand-side of the three continuity Eqs. (31), (32), and (33). This can be accomplished for each layer in the slab, since $N_e(x)$, $N_I(x)$, $N_{NI}(x)$, and $T_e(x)$ are known initially ($t = 0$). All the reaction rate coefficients are known as functions of either T or T_e. The fluxes Γ_e, Γ_I, and T_e can be determined from Eqs. (34) through (37). The spatial derivatives appearing in Eqs. (31) through (36) are calculated numerically by fitting cubic splines (Wendroff, 1966) to the original data giving N_e, T_e, N_I, and N_{NI} at $t = 0$. Then, the splines may be differentiated explicitly to obtain very accurate formulas for the derivatives. Once all the quantities on the right-hand-side of Eqs. (31) through (33) have been evaluated numerically for $t = 0$, these three continuity equations can be integrated one small step forward in time. This completes the third stage. The whole process is repeated starting at the first stage.

The computer program for calculating the nonlinear transmission and reflection coefficients of a reentry plasma consists of a main program that calls into play about 25 subroutines. The three stages in the numerical solution procedure are accomplished in three computer subroutines. Except for the ionization frequency ν_I, the effective collision frequency ν_{eff}, and the normalized effective plasma frequency ρ, all the plasma transport coefficients are evaluated at each step of the numerical solution by calling separate computer subroutines.

The data that is read into the main program consists of the initial conditions $N_e(x, t = 0)$, $N_I(x, t = 0)$, $N_{NI}(x, t = 0)$, $T_e(x, t = 0)$, the transmitted field intensities E_y $(x = L, t = 0)$, $H_z(x = L, t = 0)$, the neutral gas temperature and composition $T(x)$, $N_2(x)$, $O_2(x)$, $N(x)$, $O(x)$, $NO(x)$, and NATA (x), where NATA (x) is the electronegative additive density profile in the x-direction. In addition, data from the separate Boltzmann equation program is first processed and then read into the main part of the nonlinear transmission program. The processing is done in order to improve the efficiency and running time of the nonlinear transmission program.

This data processing consists of the following procedures. The data output from the Boltzmann equation program is made up of two-dimensional arrays: $T_e(x_i, E_k)$, $\nu_I(x_i, E_k)$, $\nu_{eff}(x_i, E_k)$, and $\rho(x_i, E_k)$ where $i = 1, \ldots, M$ and $k = 1, \ldots, N$. Now, during the course of a calculation, a value of T_e may be required at some intermediary position between x_i and x_{i+1} and at some intermediary field intensity between E_k and E_{k+1}. The intermediate values of T_e are obtained by spline interpolation. Since the original data output T_e (x_i, E) is such that the points x_1, x_2, and $\ldots x_m$ and the points E_1, $E_2, \ldots E_N$ are not equally spaced, the data is initialized by spline interpolation in x and in E so that the E values become equally spaced. The spline interpolation of the data T_e, ν_I, ν_{eff}, and ρ in terms of the E- and x-values serves two purposes: (1) the E-values become equally spaced, so that $h_E = E_{i+1} - E_i$ is a constant, therefore, further interpolation in E becomes very efficient; (2) the step size $h = x_{i+1} - x_i$ can be made initially very small, which greatly increases the accuracy of the Runge-Kutta integration of Maxwell's equations.

Once the data has been initialized so that the E-values are equally spaced, and h is small, then further interpolation of T_e, ν_I, ν_{eff}, or ρ is never required in terms of the x-values and interpolation in terms of E-values is efficient. However, during the course of tne calculations, the values of T_e, ν_I, ν_{eff}, and ρ will be required at arbitrary values of E. Hence, interpolation of the data will always be required in terms of the E values. Nevertheless, it still pays to initialize the data by spline interpolation so that the E values also become equally spaced, that is, $h_E = E_{k+1} - E_k$ is a constant. This is due to the fact that further spline interpolation of the data in terms of the E values is much more rapid and efficient when the data points are equally spaced. This fact may be demonstrated by considering the properties of a spline.

Consider a set of data $(y_1, y_2, \ldots y_m)$ given at the points $(x_1, x_2, \ldots x_m)$. A cubic spline can be fit to these points by connecting each pair of adjacent points with a section of a third-degree polynomial and then matching up the sections so that the first and second derivatives are continuous at each point. If Z_i is the value of the second derivative at the point $i = 1, 2, \ldots M$, then between the points (x_k, y_k) and (x_{k+1}, y_{k+1}) the second derivative has the value:

$$S'' = Z_k\left(\frac{x_{k+1}-x}{d_k}\right) + Z_{k+1}\left(\frac{x-x_k}{d_k}\right) \tag{38}$$

where $d_k = x_{k+1} - x_k$, and $S(x)$ is the spline curve. Integrating this formula twice and requiring that the spline pass through the points (x_k, y_k) and (x_{k+1}, y_{k+1}) yields the formula for a cubic spline:

$$S(x) = Z_k \frac{(x_{k+1}-x)^3}{6 \cdot d_k} + Z_{k+1} \frac{(x-x_k)^3}{6 \cdot d_k} + (x_{k+1}-x)\left(\frac{y_k}{d_k} - \frac{Z_k d_k}{6}\right)$$
$$+ (x-x_k)\left(\frac{y_{k+1}}{d_k} - \frac{Z_{k+1} d_k}{6}\right) . \tag{39}$$

In Eq. (39), all the quantities are known except the spline coefficients Z_k and Z_{k+1}. One condition that must be satisfied is that the derivative of the spline S' at the point (x_k, y_k), according to Eq. (39), must be the same as that determined by the corresponding formula for the interval (x_{k-1}, y_{k-1}) to (x_k, y_k). This condition yields the basic continuity equation for the spline coefficients at the interior points $k = 2, 3, \ldots M-1$,

$$Z_{k-1}\left(\frac{d_{k-1}}{6}\right) + Z_k\left(\frac{d_{k-1}+d_k}{3}\right) + Z_{k+1}\left(\frac{d_k}{6}\right) = \left(\frac{y_{k+1}-y_k}{dk}\right) - \frac{(y_k-y_{k-1})}{d_{k-1}} . \tag{40}$$

The two additional conditions at the end points x_1 and x_m may be taken as

$$Z_1 = Z_m = 0 . \tag{41}$$

Conditions given in Eq. (41) define a natural spline. A natural spline satisfies the condition that its mean square curvature is the least, so that the natural spline is the smoothest of all interpolating functions. Also, for natural splines, as the number of interpolating points approaches infinity, $S(x)$ approaches $y(x)$ uniformly and $S'(x)$ approaches $y'(x)$ uniformly (Wendroff, 1966).

The set of spline coefficients defined by Eqs. (40) and (41) satisfy a linear system of tridiagonal equations.

The solution to the tridiagonal system of equations of the form

$$a_k Z_{k-1} + b_k Z_k + c_k Z_{k+1} = d_k \tag{42}$$

may be readily obtained assuming

$$Z_{k-1} = p_k Z_k + q_k \, . \tag{43}$$

Substituting Eq. (43) into Eq. (42) yields

$$p_{k+1} = -c_k / (a_k p_k + b_k) \tag{44}$$

and

$$q_{k+1} = (d_k - a_k q_k) / (a_k p_k + b_k) \, . \tag{45}$$

For the system given in Eq. (40), this yields

$$p_{k+1} = - (d_k/6) \Big/ \left[\left(\frac{d_{k-1}}{6} \right) p_k + \left(\frac{d_{k-1} + d_k}{3} \right) \right] \tag{46}$$

$$q_{k+1} = - \left[(y_{k+1} - y_k)/d_k - (y_k - y_{k-1})/d_{k-1} - \left(\frac{d_{k-1}}{6} \right) q_k \right] (p_{k+1}) \left(\frac{6}{d_k} \right) \, . \tag{47}$$

with the end conditions given by Eq. (41), $p_1 = p_2 = q_1 = q_2 = 0$ and $Z_{m-1} = q_m$.

For equally spaced data points, the spline curve given by Eq. (39) takes the simple form:

$$S(x) = \bar{Z}_k (\bar{x}_{k+1} - \bar{x})^3 + \bar{Z}_{k+1} \cdot (\bar{x} - \bar{x}_k)^3 + (\bar{x}_{k+1} - \bar{x})(y_k - \bar{Z}_k) + (\bar{x} - \bar{x}_k)(y_{k+1} - \bar{Z}_{k+1}) \tag{48}$$

where

$d_k = h = x_{k+1} - x_k$

$h = \text{const.}$

$\bar{x}_k = x_k/h$

$\bar{x} = x/h$

$\bar{Z}_k = Z_k h^2/6$.

For such equally spaced data points, the p_{k+1} and q_{k+1} coefficients become:

$$p_{k+1} = -1/(4 + p_k) \tag{49}$$

$$q_{k+1} = -p_{k+1}(y_{k+1} - 2y_k + y_{k-1} - q_k) . \tag{50}$$

Not only are the expressions for p_k and q_k much simpler in the case of equally spaced data points, the p_k coefficients given by Eq. (49) are universal constants, independent of the data! Thus, the spline coefficients and the formula for the spline can be calculated very efficiently for equally spaced points.

The formula for the derivative of the spline is given by

$$S'(x) = 1/h \left[-3\bar{Z}_k(\bar{x}_{k+1} - \bar{x})^2 + 3\bar{Z}_{k+1}(\bar{x} - \bar{x}_k)^2 - (y_k - \bar{Z}_k) + (y_{k+1} - \bar{Z}_{k+1}) \right] . \tag{51}$$

This derivative formula is used to numerically differentiate the quantities $N_e T_e$, $N_I T$, and $N_{NI} T$ that appear on the RHS of Eqs. (34) through (36) for Γ_e, Γ_I, and Γ_{NI}. However, formulas (49) and (50) for p_k and q_k are not suitable for use in formula (51) for differentiating the fluxes Γ_e, Γ_I, and Γ_{NI} that appear on the RHS of Eqs. (31) through (33). This is due to the boundary conditions at the catalytic wall x = 0, where $N_e = N_I = N_{NI} = 0$ for all time. This implies that $\frac{\partial \Gamma_e}{\partial x} = \frac{\partial \Gamma_i}{\partial x} = \frac{\partial \Gamma_{NI}}{\partial x} = 0$ at x = 0. Since the natural spline S and its derivative S' are defined in terms of the spline coefficients given by Formulas (43), (49), and (50), where the spline coefficients are defined so that S'' = 0 at x = 0 and x = L, then it is necessary to redefine the spline coefficients and the formulas for p_k and q_k so that S' = 0 at x = 0 and x = L, instead of S'' = 0.

Thus, for a spline S which is defined so that $S' = 0$ at $x = 0$ and $x = x_m$, formulas (40), (48), and (51) remain unchanged. However, the end conditions of Eq. (41) become

$$-Z_2 - 2Z_1 = y_1 - y_2 \tag{52}$$

and

$$2Z_m + Z_{m-1} = -y_m + y_{m-1} \tag{53}$$

so that now $p_1 = 0$, but

$$p_2 = -0.5 \tag{54}$$

and

$$p_{k+1} = -1/(p_{k+4}) \tag{55}$$

for $m > k \geq 2$, and $p_k = 0$ for $k > m$. Also $q_1 = 0$, but

$$q_2 = 0.5(y_2 - y_1) \tag{56}$$

and

$$q_{k+1} = -p_{k+1}(y_{k+1} - 2y_k + y_k - q_k) \tag{57}$$

for $m > k \geq 2$. For

$$k = m + 1,\ q_{m+1} = (-y_m + y_{m-1} - q_m)/(p_m + 2) \tag{58}$$

and $q_k = 0$ for $k > m+1$. Then,

$$Z_m = q_{m+1} \tag{59}$$

and

$$Z_{k-1} = p_k Z_k + q_k \tag{60}$$

for $m \geq k \geq 2$.

As in the case of the natural spline, the p_k coefficients are independent of the data.

The first stage of the numerical procedure is the integration of Maxwell's Eqs. (27) through (30), using a fourth-order Runge-Kutta procedure. Values of the electric and magnetic field are assumed on the transmitted face of the slab ($x = L$), such that

$$Z_0 = 377.\ \text{ohms} = E_y\,(x=L)/H_z\,(x=L)\ . \tag{61}$$

Each step in the Runge-Kutta integration corresponds to a thin plasma layer of thickness h, over which the values of E_y, H_z, T_e, ν_I, ν_{eff}, ρ, ν_{DR}, ν_{AT}, N_e, N_I, and N_{NI} do not vary. The step size h is about 0.001, so that the error is about 10^{-12} (error $\approx h^4$).

The first stage of the numerical procedure at time $t = 0$ requires only a single backward integration through the slab, where the values of T_e and all the transport coefficients are calculated and stored at each step. Subsequent first stage and second stage procedures, after the continuity equations have been integrated one or more steps forward in time, require iterated backward then forward integrations of Maxwell's equations. As explained previously, the backward integrations are required to calculate the reflection coefficient R, the transmission coefficient TR, and the complex impedance Z. The forward integrations calculate the field distribution and the variation of the dielectric constant K with distance x. The iterations on the spatial integrations are continued until the successive forward integrations differ by less than a preassigned tolerance.

The Runge-Kutta formula used for a system of coupled nonlinear first-order equations is of the form

$$\frac{dY^i}{dx} = F^i(x, Y^1, Y^2, \ldots Y^N) \tag{62}$$

is given by (Hildebrand, 1956):

$$Y^i_{n+1} = Y^i_n + \frac{1}{6}\,(k^i_0 + 2k^i_1 + 2k^i_2 + k^i_3) \tag{63}$$

where

$$k^i_0 = h F^i(x_n, Y^1_n, Y^2_n, \ldots Y^N_n)$$

$$k^i_1 = h F(x_n + \tfrac{1}{2}h,\ Y^1_n + Y_2 k^1_0,\ Y^2_n + \tfrac{1}{2}k^2_0,\ \ldots\ Y^N_n + \tfrac{1}{2}k^N_0)$$

$$k_2^i = hF(x_n + \tfrac{1}{2}h, Y_n^1 + \tfrac{1}{2}k_1^1, Y_h^2 + \tfrac{1}{2}k_1^2 \ldots Y_n^N + \tfrac{1}{2}k_1^N)$$

$$k_3^i = hF(x_n + \tfrac{1}{2}h, Y_n^1 + k_2^1, Y_n^2 + k_2^2, \ldots Y_n^N + k_2^N) .$$

Here, $i = 1, 2 \ldots N$

h = step size = $x_{k+1} - x_k$

Y_n^i = i^{th} dependent variable at n^{th} step

and

x_n = independent variable at n^{th} step.

After each backward integration of Maxwell's equations, the reflection and transmission coefficients, R and TR, and the complex impedance of the plasma Z can be calculated according to the formulas:

$$R = \frac{Z - Z_o}{Z + Z_o} \tag{64}$$

$$T_R = \frac{(1+R)\, E_y(x=L)}{E_y(x=0)} \tag{65}$$

and

$$Z = \frac{E_y(x=0)}{H_z(x=0)} \quad . \tag{66}$$

After the very first backward integration at time $t = 0$, the incident electric field E_{INC} may be calculated according to the formula:

$$E_{INC} = \frac{E_y(x=0)}{(1+R)} . \tag{67}$$

At subsequent time increments, after $t = 0$, the total electric field at the incident face of the slab $E_y(x=0)$ is calculated after each backward integration and before each forward integration:

$$E_y(x=0) = (1+R)\, E_{INC} \; . \tag{68}$$

The total magnetic field at the incident face of the slab may be calculated according to the formula

$$H_z(x=0) = E_y(x=0)/Z \; . \tag{69}$$

Then, these values of E_y and H_z may be used to start the forward integration of Maxwell's equations through the slab. At each step in the forward integration process, the total electric field amplitude is calculated and used to determine the value of the complex dielectric constant K(x) in each thin layer. The value of K as a function of x is then used in the subsequent backward integration procedure.

The third stage in the numerical procedure involves the integration of continuity Eqs. (31) through (33) one small step forward in time, h_t. This integration is achieved by using the Runge-Kutta fourth-order formula given in Eq. (63).

4. CONCLUSIONS

The maximum error on the spline interpolation and the spline differentiation formulas is proportional to h^2, where h = step size in spline interpolation (Wendroff, 1966):

$$\max\left| f(x)-S(x)\right| \leq \frac{M}{\sqrt{120}} \left| b-a\right|^2 h^2 \tag{70}$$

$$\max\left| f'(x)-S'(x) \right| \leq \frac{M}{\sqrt{120}}\left| b-a\right| h^2 , \tag{71}$$

Here,

f(x)	=	original function
S(x)	=	spline fit of f(x)
a	=	lower end of interval
b	=	upper end of interval
M	=	$\max \left\|f^{IV}(x)\right\|$
h	=	step size.

In the numerical differentiations performed in Eqs. (31) through (36), the maximum interpolation error can be made less than 0.1 percent if the reentry plasma slab is divided into 100 layers or more.

The error in the Runge-Kutta fourth-order integration is proportional to h^4. If the reentry plasma slab is divided into 100 layers, then the error in the Runge-Kutta formula is about 10^{-8} or less. Thus, the error bounds on the numerical interpolation, differentiation, and integration can all be made quite small, much less than the error in the values of the reaction-rate coefficients.

The techniques for numerically calculating the nonlinear reflection and transmission coefficients presented in this report are restricted to the case of a plane wave at normal incidence to the plasma slab. The results can be readily extended to the case of oblique incidence, provided the electric vector of the incident wave is normal to the plane of incidence. However, if there is a component of the electric vector in the plane of incidence, then longitudinal waves can be launched into the plasma. At high power levels, the longitudinal waves can excite a host of parametric instabilities and give rise to an anomalous resistivity of the plasma (Goldman and Dubois, 1972).

The curves of transmitted power vs time will most likely be similar in shape to the curves presented in the report by Fante and Mayhan, (1971), even when electronegative compounds are injected into the reentry plasma, with the important difference that the transmitted power level will increase as the percentage of chemical additive increases.

The computer program that has been developed will permit a large number of various electronegative gases to be tested for their capability to increase the transmission coefficient of reentry plasmas at high electromagnetic wave power levels.

References

Bakshi, P.M., Haskell, R.E., and Papa, R.J. (1968) Can. J. Phys. 46:1547.

Carlton, N.P. and Megill, L.R. (1962) Phys. Rev. 126:2089.

Epstein, M. (1965) Rept No. TDR-669 (6240-20)-1, Aerospace Corporation.

Epstein, M. (1968) Phys. Fluids 11:896.

Epstein, M. (1969) Rpt No. TR-0066 (5240-20)-2, Aerospace Corp.

Epstein, M. and Lenander, C.J. (1968) Phys. Fluids 11:2753.

Fante, R.L. (1971) J. Appl. Phys. 42:4202.

Fante, R.L. and Mullin, C.R. (1965) Proc. IEEE 53:484.

Fante, R.L. and Mayhan, J.T. (1971) AFCRL-71-0334, Contract No. F19628-69-C-0121.

Goldman, M.V. and Dubois, D.F. (1972) AFWL-TR-72-101, Contract No. F29601-71-C-0052.

Hildebrand, F.B. (1956) Introduction to Numerical Analysis, McGraw-Hill.

Lenander, C.J. (1968a) Rpt No. TR-0158 (3240-20)-17, Aerospace Corp.

Lenander, C.J. (1968b) SAMSO-TR-68-409, Aerospace Corp.

Lew, H.G. (1970) AFCRL-70-0702, G.E. Rpt. under contract F19628-69-C-0112.

Lew, H.G. (1972) private communication.

Light, G.C. and Taylor, E.C. (1968) J. Appl. Phys. 39:1591.

Macdonald, A.D. (1966) Microwave Breakdown in Gases, Wiley, New York.

MacDonald, A.D., Gaskell, D.V., and Gitterman, H.N. (1963) Phys. Rev. 130:1841.

Mayhan, J.T. (1969) IEEE Trans. Antennas Propagation 17:251.

Mayhan, J.T. and DeVore, R.V. (1968) J. Appl. Phys. 39:5746.

Mayhan, J.T. and Fante, R.L. (1969) J. Appl. Phys. 40:449.

Mayhan, J.T. and Yos, J.M. (1969) AVCO AVSD-0374-69-CR Vol 1.

Papa, R.J. and Case, C.T. (1965) Can. J. Phys. 43:2021, 2036.

Pergament, H.S., Mikatarian, R.R., and Kurzius, S.C. (1972) AIAA Paper No. 72-670.

Shkarofsky, I.P., Bachynski, M.P., and Johnston, T.W. (1961), Electromagnetic Effects of Reentry, edited by W. Rotman and G. Meltz, Pergamon Press, p. 24.

Taylor, W.C., Chown, J.B., and Morita, T. (1968) J. Appl. Phys. 39:191.

Taylor, W.C., Sharfman, W.E., and Morita, T. (1971) Voltage breakdown of microwave antennas in Advances in Microwaves, 7:59.

Wendroff, B. (1966) Theoretical Numerical Analysis, Academic Press.

Whitmer, R.F. and Herrman, G.F. (1966) Phys. Fluids 9:768.